NASA/TM-2006-214532

Simulation of Delamination Propagation in Composites Under High-Cycle Fatigue by Means of Cohesive-Zone Models

Albert Turon
Escola Politècnica Superior, Universitat de Girona, Girona, Spain

Josep Costa
Escola Politècnica Superior, Universitat de Girona, Girona, Spain

Pedro P. Camanho
Faculdade de Engenharia, Universidade do Porto, Porto, Portugal

Carlos G. Dávila
Langley Research Center, Hampton, Virginia

December 2006

The NASA STI Program Office . . . in Profile

Since its founding, NASA has been dedicated to the advancement of aeronautics and space science. The NASA Scientific and Technical Information (STI) Program Office plays a key part in helping NASA maintain this important role.

The NASA STI Program Office is operated by Langley Research Center, the lead center for NASA's scientific and technical information. The NASA STI Program Office provides access to the NASA STI Database, the largest collection of aeronautical and space science STI in the world. The Program Office is also NASA's institutional mechanism for disseminating the results of its research and development activities. These results are published by NASA in the NASA STI Report Series, which includes the following report types:

- TECHNICAL PUBLICATION. Reports of completed research or a major significant phase of research that present the results of NASA programs and include extensive data or theoretical analysis. Includes compilations of significant scientific and technical data and information deemed to be of continuing reference value. NASA counterpart of peer-reviewed formal professional papers, but having less stringent limitations on manuscript length and extent of graphic presentations.

- TECHNICAL MEMORANDUM. Scientific and technical findings that are preliminary or of specialized interest, e.g., quick release reports, working papers, and bibliographies that contain minimal annotation. Does not contain extensive analysis.

- CONTRACTOR REPORT. Scientific and technical findings by NASA-sponsored contractors and grantees.

- CONFERENCE PUBLICATION. Collected papers from scientific and technical conferences, symposia, seminars, or other meetings sponsored or co-sponsored by NASA.

- SPECIAL PUBLICATION. Scientific, technical, or historical information from NASA programs, projects, and missions, often concerned with subjects having substantial public interest.

- TECHNICAL TRANSLATION. English-language translations of foreign scientific and technical material pertinent to NASA's mission.

Specialized services that complement the STI Program Office's diverse offerings include creating custom thesauri, building customized databases, organizing and publishing research results ... even providing videos.

For more information about the NASA STI Program Office, see the following:

- Access the NASA STI Program Home Page at ***http://www.sti.nasa.gov***

- E-mail your question via the Internet to help@sti.nasa.gov

- Fax your question to the NASA STI Help Desk at (301) 621-0134

- Phone the NASA STI Help Desk at (301) 621-0390

- Write to:
  NASA STI Help Desk
  NASA Center for AeroSpace Information
  7115 Standard Drive
  Hanover, MD 21076-1320

NASA/TM-2006-214532

Simulation of Delamination Propagation in Composites Under High-Cycle Fatigue by Means of Cohesive-Zone Models

Albert Turon
Escola Politècnica Superior, Universitat de Girona, Girona, Spain

Josep Costa
Escola Politècnica Superior, Universitat de Girona, Girona, Spain

Pedro P. Camanho
Faculdade de Engenharia, Universidade do Porto, Porto, Portugal

Carlos G. Dávila
Langley Research Center, Hampton, Virginia

National Aeronautics and
Space Administration

Langley Research Center
Hampton, Virginia 23681-2199

December 2006

Available from:

NASA Center for AeroSpace Information (CASI)
7115 Standard Drive
Hanover, MD 21076-1320
(301) 621-0390

National Technical Information Service (NTIS)
5285 Port Royal Road
Springfield, VA 22161-2171
(703) 605-6000

Simulation of Delamination Propagation in Composites under High-Cycle Fatigue by means of Cohesive-Zone Models

A. Turon [a], J. Costa [a], P.P. Camanho [b], C.G. Dávila [c]

[a] *AMADE, Polytechnic School, University of Girona, Campus Montilivi s/n, 17071 Girona, Spain*

[b] *DEMEGI, Faculdade de Engenharia, Universidade do Porto, Rua Dr. Roberto Frias, 4200-465, Porto, Portugal*

[c] *NASA Langley Research Center, Hampton, Virginia, U.S.A.*

Abstract

A damage model for the simulation of delamination propagation under high-cycle fatigue loading is proposed. The basis for the formulation is a cohesive law that links fracture and damage mechanics to establish the evolution of the damage variable in terms of the crack growth rate dA/dN. The damage state is obtained as a function of the loading conditions as well as the experimentally-determined coefficients of the Paris Law crack propagation rates for the material. It is shown that by using the constitutive fatigue damage model in a structural analysis, experimental results can be reproduced without the need of additional model-specific curve-fitting parameters.

Key words: Delamination, Fatigue, Cohesive elements.

1 Introduction and motivation

High-cycle fatigue is a common cause of failure in aerospace structures. In laminated composite materials, the fatigue process involves several damage mechanisms that result in the degradation of the structure. One of the most important fatigue damage mechanisms is interlaminar damage (delamination).

There are two basic approaches for the analysis of delamination under fatigue loading: Fracture Mechanics and Damage Mechanics. Fracture Mechanics relates the fatigue crack growth rate with the amplitude of the energy release

rate and mode-ratio. In most studies, fatigue crack growth rates are described with the Paris Law [1,2]:

$$\frac{\partial A}{\partial N} = C\left(\frac{\Delta G}{G_c}\right)^m \tag{1}$$

where A is the crack area, N is the number of cycles, and the parameters C and m depend on the mode-ratio and must be determined experimentally. The cyclic variation of the energy release rate, ΔG, depends on the loading conditions, and G_c is the fracture toughness of the material. Alternatively, the crack growth rate may be expressed in terms of the stress intensity factor range, ΔK, or the J-integral range ΔJ [3,4].

Damage Mechanics Models describe the loss of a material's ability to carry loads by using one or more damage variables. In this paper, a Damage Mechanics formulation is adopted in which fracture is represented by a cohesive zone model (CZM) that uses a single damage variable. The material separation under cyclic loading is described by a constitutive equation formulated in the context of the thermodynamics of irreversible processes. Within an irreversible cohesive zone model, material separation is described as a relationship between crack surface traction and separation across the crack.

Under general cyclic loading, the total damage is the sum of the damage caused by static or quasi-static loads and the damage that results from the cyclic loads. There are several models that extend cohesive laws for monotonic loading into forms suitable for cyclic loading. Yang et al. [5] developed a cohesive law that describes separately the unloading and reloading processes and creates a hysteresis loop between unloading and reloading paths. Roe and Siegmund [6] describe fatigue crack growth by incorporating a damage evolution equation for cyclic loading. Nguyen et al. [7] developed a cohesive zone model for cyclic loads in which the irreversible material degradation is represented as a loss of stiffness in the cohesive zone during the unloading portion of the load cycle. Similarly, Goyal-Singhal et al. extended the capability of their cohesive-decohesive constitutive model [8] to account for fatigue damage accumulation during unloading [9]. In all of these references, the fatigue damage accumulation is accounted for in a cycle-by-cycle analysis. For high-cycle fatigue, where the number of cycles considered is larger than 10^5, a cycle-by-cycle analysis would be computationally intractable.

For high-cycle fatigue, the damage evolution that results from cyclic loads is usually formulated as a function of the number of cycles and strains (or displacement jumps) [10–12]. In these references, a damage evolution law expressed in terms of the number of cycles is established a priori by adjusting several parameters through a trial-and-error calibration of the analysis.

In this paper, an approach is proposed whereby the evolution of damage derives from a Fracture Mechanics description of the fatigue crack growth rate. The approach is formulated using the cohesive zone model concept. A constitutive damage model previously developed by the authors for static or quasi-static loads [14] is enhanced to incorporate a damage evolution law for high-cycle fatigue.

In the present model for fatigue damage, the evolution of the damage variable associated with cyclic loading is derived from a Fracture Mechanics description of the fatigue crack growth rate. Therefore, the proposed model is based on linking Fracture Mechanics and Damage Mechanics. The model relates damage accumulation to the number of load cycles while taking into account the loading conditions (load ratio, R, energy release rate, G, and fracture mode mixity). When used in a structural analysis, the model can simulate the dependence of the crack growth rate on these parameters. In addition to the Paris Law crack growth regime, the model also exhibits a threshold value for no growth as well as quasi-static tearing. The new fatigue damage model is implemented as a user-written element in ABAQUS [37] based on the cohesive finite element previously developed by the authors [14].

2 Cohesive zone model approach

The CZM approach [15–17] is one of the most commonly used tools to simulate interfacial fracture. The CZM approach assumes that a cohesive damage zone develops near the tip of a crack.

As mentioned above, cohesive damage zone models relate tractions, τ, to displacement jumps, $\bar{\Delta}$, at an interface where a crack may occur. Damage initiation is related to the interfacial strength, τ^o. When the area under the traction-displacement jump relation is equal to the fracture toughness, G_c, the traction is reduced to zero and new crack surfaces are formed. If a linear softening law is used, the new crack surfaces are completely formed when the displacement jump is equal to, or greater than, the final displacement jump, $\bar{\Delta}^f$ (see Figure 1):

$$\begin{cases} \tau = (1 - \bar{\mathsf{d}})\tau^o & \bar{\Delta} < \bar{\Delta}^f \\ \tau = 0 & \bar{\Delta} \geq \bar{\Delta}^f \end{cases} \tag{2}$$

In the cohesive damage model, the damage variable $\bar{\mathsf{d}}$ describes the density of microcracks of a representative element surface. Then, the damage variable

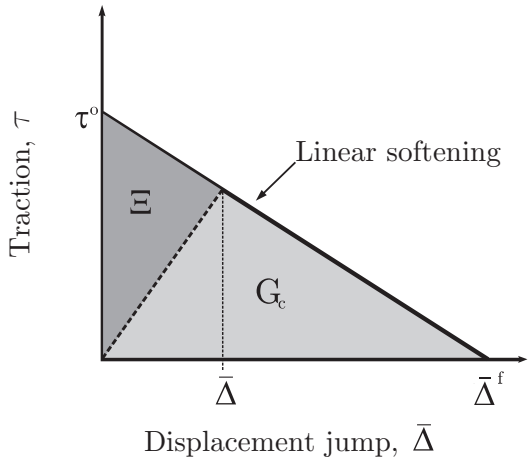

Fig. 1. *Linear softening law for a cohesive zone model approach.*

can be interpreted as the ratio of the damaged area, A_{d}, with respect to the area A^e associated with the local discretization [18]. In the context of finite elements, the area A^e represents the area of the element (or that of an integration point). Using the linear softening law represented in Figure 1, this ratio is a function of the energy dissipated during the damage process, Ξ, and of the critical energy release rate, G_c. Using Equation (2), the damage variable can be expressed as the ratio between the current and the final displacement jumps:

$$\bar{\mathsf{d}} = \frac{A_{\mathsf{d}}}{A^e} = \frac{\Xi}{G_c} = \frac{\bar{\Delta}}{\bar{\Delta}^f} \tag{3}$$

2.1 Numerical representation of the CZM

Cohesive finite elements have been developed to capture the initiation and propagation of delamination cracks [8,13,14,19–28]. As in most other cohesive element formulations, the constitutive law used in this paper is a bilinear relation between the tractions and the displacement jumps [13,14,26,29]. The bilinear cohesive law is similar to the softening law of the CZM but with an initial linear elastic response before damage initiation, as shown in Figure 2. This linear elastic part is defined using a penalty stiffness parameter, K, that ensures a stiff connection between the surfaces of the material discontinuity. The interfacial strength and the penalty stiffness define an onset displacement jump, Δ^o, related to the initiation of damage. The equivalence between the constitutive equations of the physical cohesive zone model and the numerical constitutive equations is shown in Figure 2.

The next section describes the kinematics and constitutive relation of cohesive

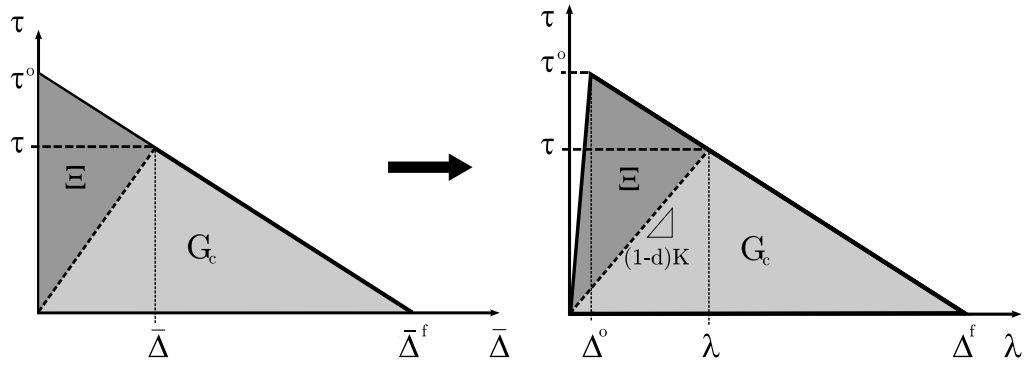

Fig. 2. *Traction-displacement laws describing the physical (left) and numerical (right) constitutive equations of the CZM.*

zone models for quasi-static loading that are also the foundation of the fatigue damage model proposed in this paper.

3 Kinematics and constitutive model for quasi-static loading

The displacement jump across the interface $[\![u_i]\!]$, is obtained from the displacements of the points located on the top and bottom sides of the interface, u_i^+ and u_i^-, respectively:

$$[\![u_i]\!] = u_i^+ - u_i^- \tag{4}$$

where $u_i^\pm$ are the displacements with respect to a fixed Cartesian coordinate system. A co-rotational formulation is used to express the components of the displacement jumps with respect to the deformed interface. The coordinates $\bar{x}_i$ of the deformed interface can be written as [30]:

$$\bar{x}_i = X_i + \frac{1}{2}\left(u_i^+ + u_i^-\right) \tag{5}$$

where X_i are the coordinates of the undeformed interface.

The components of the displacement jump tensor in the local coordinate system on the deformed interface, Δ_m, are expressed in terms of the displacement field in global coordinates:

$$\Delta_m = \Theta_{mi}\,[\![u_i]\!] \tag{6}$$

where Θ_{mi} is the rotation tensor, defined in [13,14].

The constitutive operator of the interface, D_{ji}, relates the element tractions, τ_j, to the displacement jumps, Δ_i:

$$\tau_j = D_{ji}\Delta_i \tag{7}$$

The constitutive relations of cohesive zone models must compute accurately the energy dissipated in the process of fracture. Under single-mode loading, controlled energy dissipation is achieved by ensuring that the area under the traction-displacement jump relation equals the corresponding fracture toughness. Under mixed-mode loading, a criterion established in terms of an interaction between components of the energy release rates associated with each fracture mode is used to predict crack propagation. The formulation of the damage model previously proposed by the authors [14] is summarized in Table 1, where ψ and ψ^0 are the free energy per unit surface of the damaged and undamaged interface, respectively. The function δ_{ij} is the Kronecker delta, and the variable d is a scalar damage variable. The parameter λ is the norm of the displacement jump tensor (also called *equivalent displacement jump norm*) and it is used to compare different stages of the displacement jump state such that it is possible to define such concepts as 'loading', 'unloading' and 'reloading'. The equivalent displacement jump is a non-negative, continuous scalar function defined as:

$$\lambda = \sqrt{\langle \Delta_3 \rangle^2 + (\Delta_{shear})^2} \tag{8}$$

where $\langle \cdot \rangle$ is the MacAuley bracket defined as $\langle x \rangle = \frac{1}{2}(x + |x|)$. The displacement jump in Mode I, i.e., normal to midplane is Δ_3. The displacement jump tangent to the midplane, Δ_{shear}, is computed with the Euclidean norm of the displacement jump in Mode II and Mode III:

$$\Delta_{shear} = \sqrt{(\Delta_1)^2 + (\Delta_2)^2} \tag{9}$$

The evolution of damage is defined by a suitable monotonic scalar function, $\mathsf{G}(\cdot)$, ranging from 0 to 1. A damage consistency parameter, $\dot{\mu}$, is used to define loading-unloading conditions according to the Kuhn-Tucker relations [31]. The consistency conditions ensure that damage evolution cannot occur during unloading or neutral loading. The damage threshold for the current time, t, is r^{t}. The damage threshold is equal to the onset displacement jump, Δ^o when there is no damage at the interface. When the interface is completely damaged, the damage threshold is equal to the final displacement jump, Δ^f. In the

Table 1
Definition of the constitutive model.

Free Energy	$\psi(\Delta, \mathsf{d}) = (1-\mathsf{d})\,\psi^0(\Delta_i) - \mathsf{d}\psi^0(\delta_{3i}\langle-\Delta_3\rangle)$
Constitutive equation	$\tau_i = \frac{\partial\psi}{\partial\Delta_i} = (1-\mathsf{d})\,\delta_{ij}K\Delta_j - \mathsf{d}\delta_{ij}K\delta_{3j}\langle-\Delta_3\rangle$
Displacement jump norm	$\lambda = \sqrt{\langle\Delta_3\rangle^2 + (\Delta_{shear})^2}$
Damage criterion	$\bar{F}(\lambda^{\mathsf{t}}, r^{\mathsf{t}}) := \mathsf{G}(\lambda^{\mathsf{t}}) - \mathsf{G}(r^{\mathsf{t}}) \leq 0 \qquad \forall \mathsf{t} \geq 0$
	$\mathsf{G}(\lambda) = \frac{\Delta^f(\lambda-\Delta^o)}{\lambda(\Delta^f-\Delta^o)}$
Evolution law	$\dot{\mathsf{d}} = \dot{\mu}\frac{\partial\bar{F}(\lambda,r)}{\partial\lambda} = \dot{\mu}\frac{\partial\mathsf{G}(\lambda)}{\partial\lambda}$
Load/unload conditions	$\dot{\mu} \geq 0 \;\;;\;\; \bar{F}(\lambda^{\mathsf{t}}, r^{\mathsf{t}}) \leq 0 \;\;;\;\; \dot{\mu}\bar{F}(\lambda^{\mathsf{t}}, r^{\mathsf{t}}) = 0$
	$r^{\mathsf{t}} = \max\{\Delta^o, \max_s \lambda^s\} \quad 0 \leq s \leq \mathsf{t}$

case of crack closure during load reversal, the constitutive model is designed to prevent interpenetration of the faces of the crack by restoring the normal penalty stiffness of the element even in the presence of damage. Further details regarding the damage model used here can be found in references [13,14].

Under loading conditions, the damage variable can be obtained using the damage criterion in Table 1 as:

$$\mathsf{d} = \frac{\Delta^f(\lambda-\Delta^o)}{\lambda(\Delta^f-\Delta^o)} \tag{10}$$

In the numerical model of the CZM, the damage variable d represents a loss of stiffness and, therefore, it is not equivalent to $\bar{\mathsf{d}}$, the ratio between the damaged area, A_{d}, with respect to the area of the element, A^e, in Equation (3). Since $\bar{\mathsf{d}}$ is equal to the ratio of the energy dissipated over the fracture toughness the damaged area ratio is related to the damage variable, d, as:

$$\bar{\mathsf{d}} = \frac{A_{\mathsf{d}}}{A^e} = \frac{\Xi}{G_c} = 1 - \frac{\lambda}{\Delta^o}(1 - \mathsf{d}) \tag{11}$$

By solving Equation (10) for λ and substituting into Equation (11), the damaged area ratio becomes:

$$\frac{A_{\mathsf{d}}}{A^e} = \frac{\mathsf{d}\Delta^o}{\Delta^f(1 - \mathsf{d}) + \mathsf{d}\Delta^o} \tag{12}$$

4 Constitutive model for high-cycle fatigue

The damage evolution that results from a general loading history can be considered as the sum of the damage created by the quasi-static overloads and the damage created by the cyclic loads:

$$\dot{\mathsf{d}} = \dot{\mathsf{d}}_{static} + \dot{\mathsf{d}}_{cyclic} \tag{13}$$

The first term in the right hand side of Equation (13) is obtained from the equations presented in previous section, while the second term has to be defined to account for cyclic loading. Using a Damage Mechanics framework, several authors have formulated the damage evolution that results from cyclic loads in terms of the number of cycles and of the strains (or displacement jumps) [10–12]. These damage laws are model-specific and they are a function of several parameters that have to be adjusted to calibrate the numerical model with experimental results, usually by trial and error. In contrast, the fatigue damage model formulated here is based on a Fracture Mechanics crack growth rate characterization which is achieved by linking Fracture Mechanics and Damage Mechanics: the evolution of the damage variable, d, is related with the crack growth rate, $\frac{dA}{dN}$ as follows:

$$\frac{\partial \mathsf{d}}{\partial N} = \frac{\partial \mathsf{d}}{\partial A_{\mathsf{d}}} \frac{\partial A_{\mathsf{d}}}{\partial N} \tag{14}$$

where A_{d} is the damaged area, and $\frac{\partial A_{\mathsf{d}}}{\partial N}$ is the growth rate of the damaged area. The term $\frac{\partial A_{\mathsf{d}}}{\partial N}$ is a material property that must be characterized experimentally

for different loading conditions. The term $\frac{\partial \mathsf{d}}{\partial A_{\mathsf{d}}}$ can be obtained from Equation (12):

$$\frac{\partial \mathsf{d}}{\partial A_{\mathsf{d}}} = \frac{1}{A^e} \frac{[\Delta^f (1 - \mathsf{d}) + \mathsf{d}\Delta^o]^2}{\Delta^f \Delta^o} \tag{15}$$

4.1 Determination of the growth rate of the damaged area as a function of the number of cycles

In a degradation process involving cyclic loading, the damaged area grows as the number of cycles increase: after ΔN cycles, the damaged area ahead of the crack tip increases by $\Delta A_{\mathbf{d}}$ as schematically represented in Figure 3. It can be assumed that the increase in the crack area ΔA is equivalent to the increase in the amount of damaged area.

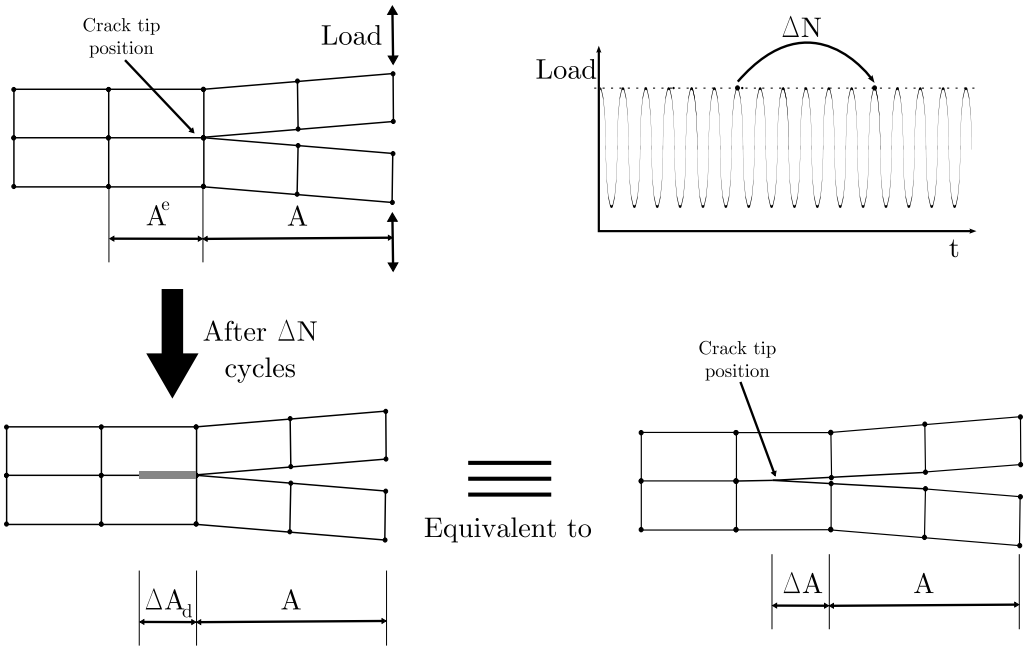

Fig. 3. *Schematic representation of the equivalence between the increase in the damaged area and the crack growth.*

The increase in the damaged area along a crack front is equal to the increase in the damaged area of all of the elements ahead of the crack tip. Therefore, the crack growth rate can be assumed to be equal to the sum of the damaged area growth rates of all damaged elements ahead of the crack tip, that is, all elements in the cohesive zone:

$$\frac{\partial A}{\partial N} = \sum_{e \in A_{\mathrm{CZ}}} \frac{\partial A_{\mathsf{d}}^{e}}{\partial N} \tag{16}$$

where A_{d}^{e} is the damaged area of one element and the term A_{CZ} is the area of the cohesive zone. Assuming that $\frac{\partial A_{\mathsf{d}}}{\partial N}$ is the mean value of the damaged area growth rate $\frac{\partial A_{\mathsf{d}}^{e}}{\partial N}$ of the elements over the cohesive zone and assuming that the mean area of the elements in the cohesive zone is A^{e}, the previous equation can be written as:

$$\frac{\partial A}{\partial N} = \sum_{e \in A_{\mathrm{CZ}}} \frac{\partial A_{\mathsf{d}}^{e}}{\partial N} = \frac{A_{\mathrm{CZ}}}{A^{e}} \frac{\partial A_{\mathsf{d}}}{\partial N} \tag{17}$$

where the ratio $\frac{A_{\mathrm{CZ}}}{A^{e}}$ represents the number of elements in which the cohesive zone has been divided. In the context of finite elements, this ratio represents the number of elements that span the cohesive zone. Rearranging terms in Equation (17), the surface damage growth rate can be written as:

$$\frac{\partial A_{\mathsf{d}}}{\partial N} = \frac{A^{e}}{A_{\mathrm{CZ}}} \frac{\partial A}{\partial N} \tag{18}$$

4.2 Evolution of the damage variable under cyclic loading

By introducing Equations (15) and (18) into Equation (14) the evolution of the damage variable as a function of the number of cycles can be written as:

$$\frac{\partial \mathsf{d}}{\partial N} = \frac{1}{A_{\mathrm{CZ}}} \frac{(\Delta^{f}(1-\mathsf{d}) + \mathsf{d}\Delta^{o})^{2}}{\Delta^{f}\Delta^{o}} \frac{\partial A}{\partial N} \tag{19}$$

The area of the cohesive zone for pure Mode I can be estimated using Rice's closed-form equation [32,33]:

$$A_{\mathrm{CZ}} = b \frac{9\pi}{32} \frac{E_{3} G^{\max}}{(\tau^{o})^{2}} \tag{20}$$

where b is the width of the delamination front, and $G^{\max}$ is taken as the maximum energy release rate in the loading cycle. E_3 is the Young's modulus

of the bulk material in the direction perpendicular to the crack plane, and τ^o is the interfacial strength.

4.3 Crack growth rate

The crack growth rate under fatigue loading, $\frac{\partial A}{\partial N}$, is a load and material-dependent characteristic that has been widely studied. The growth rate defined by the Paris Law given in Equation (1) represents crack propagation in region II of the typical pattern of the crack growth rate (see Figure 4).

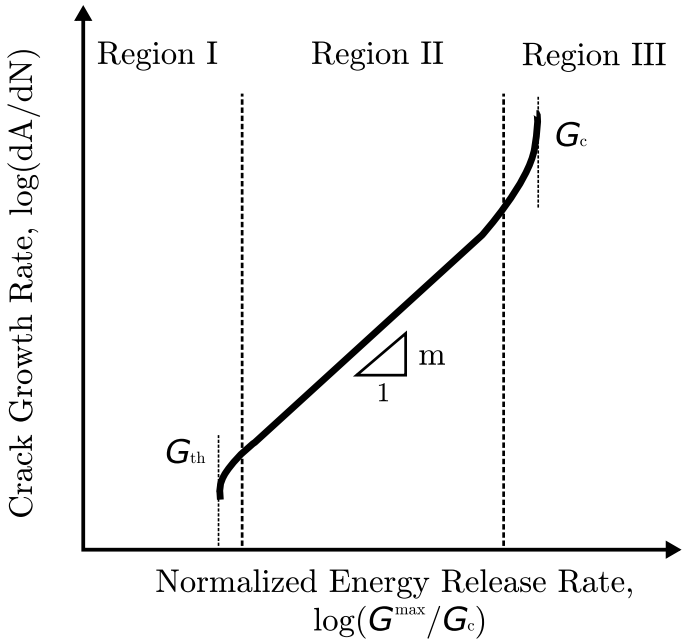

Fig. 4. *Typical crack growth rate regions.*

In region I, crack growth is not observed if the maximum energy release rate is smaller than the fatigue threshold of the energy release rate, G_{th}.

In region III, the crack growth rate increases because the maximum energy release rate approaches the fracture toughness. Tearing fracture controls the crack growth rate in region III instead of fatigue propagation.

The crack growth rate $\frac{\partial A}{\partial N}$ used in the fatigue damage model, Equation (19), is defined as a piecewise function defined as:

$$\frac{dA}{dN} = \begin{cases} C\left(\frac{\Delta G}{G_c}\right)^m \text{ , } G_{th} < G^{\max} < G_c \\ 0 \quad , \quad otherwise \end{cases} \tag{21}$$

where C, m and G_c are material constants that depend on the mode-ratio. The maximum energy release rate $G^{\max}$ and cyclic variation in the energy release rate ΔG used in the Paris Law rate equation can be computed using the constitutive law of the cohesive zone model (see Figure 5):

$$G = \int_0^{\Delta} \tau(\Delta) d\Delta \tag{22}$$

$$\Delta G = G^{\max} - G^{\min} \tag{23}$$

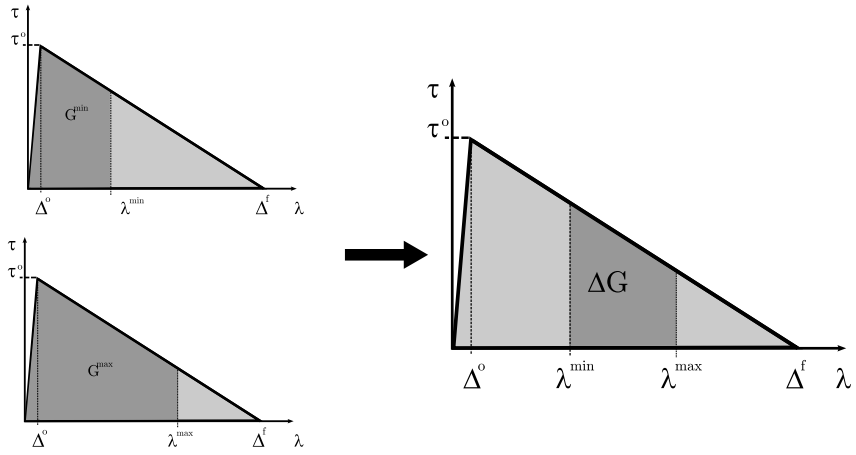

Fig. 5. *Variation of the energy release rate.*

The maximum energy release rate is:

$$G^{\max} = \frac{\tau^o}{2}\left[\Delta^o + \frac{(\Delta^f - \lambda^{\max})^2}{\Delta^f - \Delta^o}\right] \tag{24}$$

By defining the load ratio, R as:

$$R^2 = \frac{G^{\min}}{G^{\max}} \tag{25}$$

the variation of the energy release rate in Equation (23) can be re-written as:

$$\Delta G = \frac{\tau^o}{2}\left[\Delta^o + \frac{(\Delta^f - \lambda^{\max})^2}{\Delta^f - \Delta^o}\right](1 - R^2) \tag{26}$$

It is clear from Equation (26) that the model accounts for variations in the load ratio. The higher the load ratio, the smaller the variation in the energy release, as shown in Figure 6.

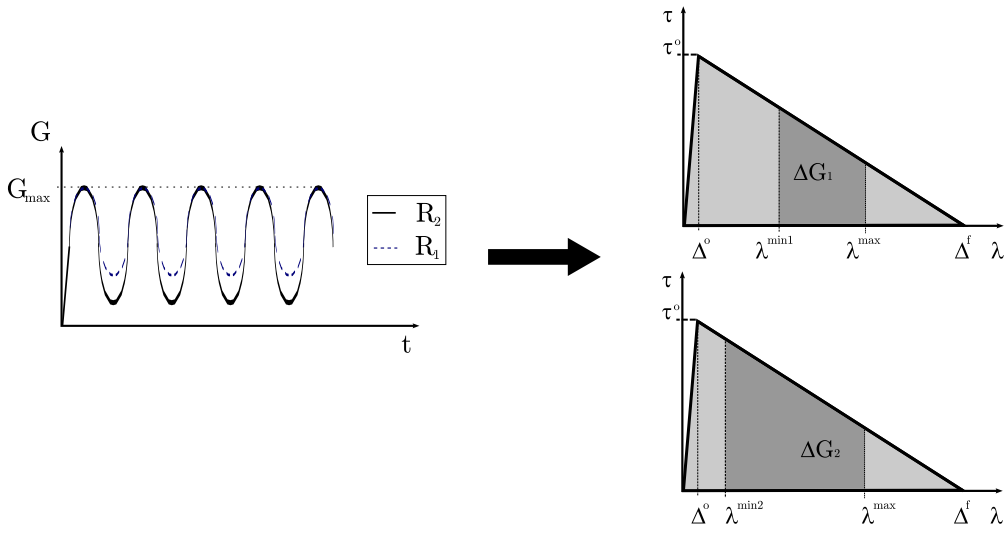

Fig. 6. *The load ratio effect is captured by the constitutive equations. The higher load ratios ($R_1 > R_2$) the smaller ΔG ($\Delta G_2 > \Delta G_1$).*

4.3.1 Mixed-mode loading

The material parameters, C, m, G_{th} used in the crack growth rate expression (21) depend on the mode ratio. In Mode I, the crack growth rate parameters are C_{I}, m_{I}, and $G_{\mathrm{I}th}$, and in Mode II, the crack growth rate parameters are C_{II}, m_{II}, and $G_{\mathrm{II}th}$. Under mixed-mode, the crack growth rate parameters C, m, and G_{th} must be determined. In this paper, the dependence of the parameters C and m on the mode ratio is assumed to be of the form[34]:

$$\log C = \log C_{\mathrm{I}} + \left(\frac{G_{\mathrm{II}}}{G_T}\right) \log C_{\mathrm{m}} + \left(\frac{G_{\mathrm{II}}}{G_T}\right)^2 \log \frac{C_{\mathrm{II}}}{C_m C_{\mathrm{I}}} \tag{27}$$

and

$$m = m_{\mathrm{I}} + m_{\mathrm{m}} \left(\frac{G_{\mathrm{II}}}{G_T}\right) + (m_{\mathrm{II}} - m_{\mathrm{I}} - m_{\mathrm{m}}) \left(\frac{G_{\mathrm{II}}}{G_T}\right)^2 \tag{28}$$

where C_{m} and m_{m} are mode-ratio material parameters that must be determined by curve-fitting experimental data.

The dependence of the energy release rate threshold is assumed to follow an expression similar to that introduced by Benzeggagh and Kenane [35] for the dependence of the Fracture Toughness with the mode-ratio:

$$G_{th} = G_{\mathrm{I}th} + (G_{\mathrm{II}th} - G_{\mathrm{I}th}) \left(\frac{G_{shear}}{G_T} \right)^{\eta_2} \tag{29}$$

where η_2 is a material parameter obtained from a curve-fit of experimental results.

4.4 Cycle jump strategy

In a degradation process involving high-cycle fatigue, a cycle-by-cycle analysis becomes computationally intractable. Therefore, a cycle jump strategy is implemented in the finite element model. A cycle jump means that the computation is done for a certain set of loading cycles at chosen intervals, and that the effect on the stiffness degradation of these loading cycles is extrapolated over the corresponding intervals in an appropriate manner. The cycle jump strategy adopted here is based on the one presented in [36]. After a certain number of cycles N_i, the damage variable d_i^J at an integration point J is computed using the quasi-static constitutive equations. The predicted evolution of the damage variable with the number of cycles, $\frac{\partial \mathsf{d}}{\partial N}$, is computed using Equation (19). The damage variable at an integration point J after ΔN_i cycles is:

$$\mathsf{d}_{i+\Delta N_i}^J = \mathsf{d}_i^J + \frac{\partial \mathsf{d}_i^J}{\partial N} \Delta N_i \tag{30}$$

To determine the number of cycles ΔN_i that can be skipped with a controlled level of accuracy, the following equation is used:

$$\Delta N_i = \frac{\Delta \mathsf{d}_{\max}}{\max\limits_J \left\{ \frac{\partial \mathsf{d}_i^J}{\partial N} \right\}} \tag{31}$$

where $\Delta \mathsf{d}_{\max}$ is a pre-established value. The smaller the choice of $\Delta \mathsf{d}_{\max}$ the higher the accuracy of the analysis.

5 Results and discussion

The present model is implemented as a user-written finite element in ABAQUS® [37] by adding the fatigue damage model to the constitutive behavior of a cohesive element previously developed in Refs. [13,14].

Several single-element tests were performed to verify the response of the fatigue damage model. Then, simulations of Mode I, Mode II and mixed-mode delamination tests were conducted to demonstrate that when the constitutive damage model is used in a structural analysis, the analysis can reproduce the response of the test specimens without the use of any model-specific adjustment parameters.

5.1 One element tests

The finite element model shown in Figure 7 is composed of two 4-node plane strain elements connected by a 4-node cohesive element representing the interface.

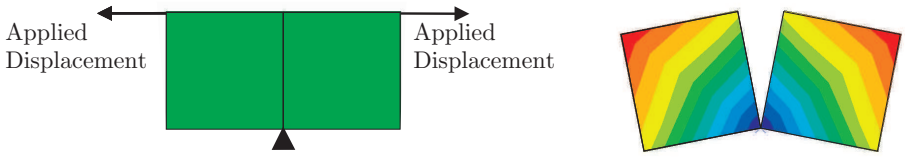

Fig. 7. *Undeformed mesh with the boundary conditions and deformed mesh of one cohesive element tests.*

The material properties shown in Table 2 correspond to a T300/977-2 carbon-fiber reinforced epoxy laminate. The Paris Law coefficients used in the simulation were $C_{\mathrm{I}} = 0.0616$ mm^2/cycle and $m_{\mathrm{I}} = 5.4$. The threshold for fatigue crack propagation was assumed to be zero.

The load was applied in two steps. The first step was a quasi-static step where the displacement jump is incremented to 20 times the onset displacement. The second step accounts for fatigue damage resulting from a maximum applied displacement of 20 times the onset displacement and a load ratio $R = 0$.

Table 2
Properties used in the models with only one cohesive element.

E_{11}	$E_{22} = E_{33}$	$G_{12} = G_{13}$	G_{23}	$\nu_{12} = \nu_{13}$	ν_{23}
150.0 GPa	11.0 GPa	6.0 GPa	3.7 GPa	0.25	0.45
G_{Ic}	G_{IIc}	τ_3^o	$\tau_2^o = \tau_1^o$	K	
0.268kJ/m^2	0.632 kJ/m^2	45 MPa	45 MPa	10^6N/mm^3	

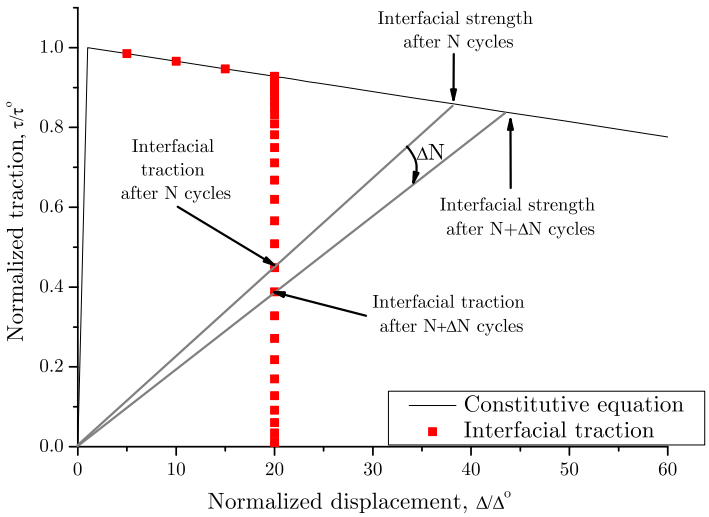

Fig. 8. *Evolution of the interface traction in the constitutive equation for a displacement jump controlled high-cycle fatigue test.*

The evolution of the interface traction in the constitutive equation for a high-cycle fatigue test under displacement control is shown in Figure 8. It can be observed that fatigue damage causes a reduction of the stiffness, the interfacial traction, and the interfacial strength. The evolution of the interface traction and strength with the number of cycles is shown in Figure 9. The shape of the obtained curves is similar to the widely-used S-N curves used in the design for fatigue strength.

5.2 Simulation of a DCB specimen under fatigue loading

Simulations of a double-cantilever beam (DCB) specimen were conducted to simulate the crack growth rate under Mode I loading for different ranges of the

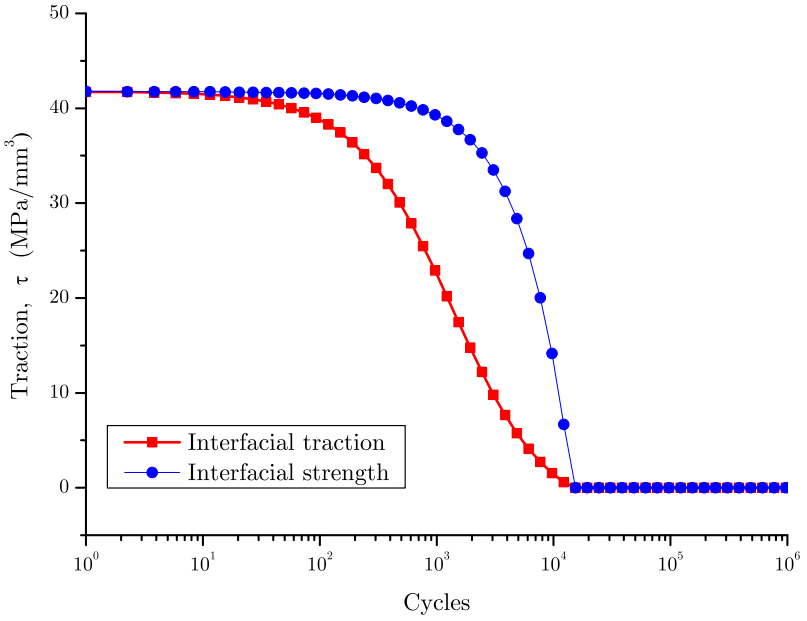

Fig. 9. *Evolution of the interface traction and the maximum interface strength as a function of the number of cycles for a displacement jump controlled high-cycle fatigue test.*

energy release rates. Experimental data on fatigue-driven delamination growth reported by Asp et al. [38] was selected for the validation of the numerical model. The specimen was fabricated with HTA/6376C carbon/epoxy prepreg produced by Hexcel. The layup consisted in $[0_{12}//(\pm 5/0_4)_S]$, where the sign // refers to the plane of the artificial delamination. The specimen was 150-mm-long, 20.0 mm-wide, with two 1.55-mm-thick arms, and an initial crack length of 35mm. A description of the experimental procedure is reported by Asp et al. [38]. The material properties are shown in Table 3 [11,38,39].

Table 3
Material properties for HTA/6376C carbon/epoxy [11,38,39].

E_{11}(GPa)	$E_{22} = E_{33}$(GPa)	$G_{12} = G_{13}$(GPa)	G_{23}(GPa)	$\nu_{12} = \nu_{13}$	ν_{23}
120	10.5	5.25	3.48	0.30	0.51
G_{Ic}(kJ/m^2)	G_{IIc}(kJ/m^2)	$\tau_2^0 = \tau_1^0$(MPa)	τ_3^0(MPa)		
0.260	1.002	30	30		

In the finite element model, the specimen's arms are loaded with opposing moments (Figure 10) to obtain a Mode I energy release rate that is independent independent of crack length and, consequently, to achieve a constant fatigue crack growth rate. The energy release rate is related to the applied moment as [11]:

$$G_{\mathrm{I}} = \frac{M^2}{bEI} \tag{32}$$

where b is the specimen width, E is the longitudinal flexural Young's modulus and I is the second moment of area of the specimen's arm.

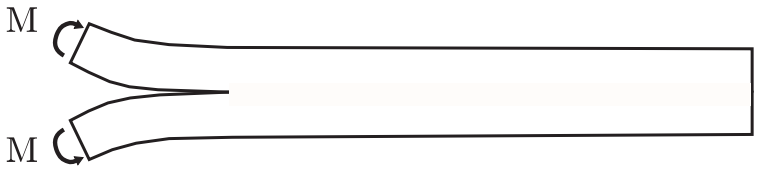

Fig. 10. *Loading pattern for Mode I specimen.*

The finite element model is composed of 4-node plane strain elements for the arms, which are connected by 4-node cohesive elements representing the interface. Two elements are used through the thickness, h, of each arm. The length of the element is 0.05mm (see Figure 11). The Paris Law parameters of Equation (1) were obtained from a linear regression of the experimental data [38]: $C_{\mathrm{I}} = 0.0616$ mm^2/cycle and $m_{\mathrm{I}} = 5.4$. The energy release rate threshold is 0.060 kJ/m^2 [38]. The material properties are shown in Table 4.

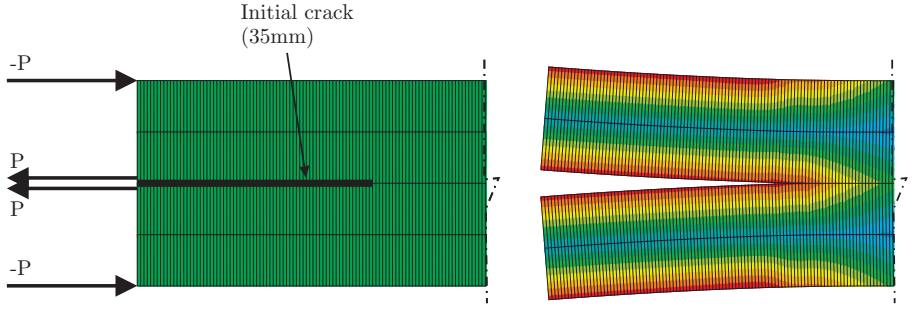

Fig. 11. *Detail of the FEM model of the DCB specimen. Two applied load P with opposite direction were applied to each arm. The applied moment is equal to the product between the applied load P and the thickness of the arm.*

The load is applied in two steps: the first analysis loading step is quasi-static and it ends at the maximum applied load. It is assumed that no fatigue damage accumulation occurs during this step. Next, a second loading step is applied

in which the maximum load is held constant, during this cycle, the analysis pseudo-time increment is assumed to be proportional to the number of loading cycles so that the fatigue damage model accounts for the accumulation of cyclic damage. The maximum variation in the damage variable $\Delta \mathsf{d}_{\max}$ allowed in a cycle jump is set to 0.001.

Table 4
Fatigue material properties for HTA/6376C carbon/epoxy obtained from references [11,39] and using Equations (27) to (29).

C_{I} (mm/cycle)	C_{II} (mm/cycle)	$C_{50\%}$ (mm/cycle)	m_{m} (mm/cycle)
0.0616	2.99	4.23	458087
m_{I}	m_{II}	$m_{50\%}$	C_{m}
5.4	4.5	6.41	4.94
G_{Ith} (kJ/m^2)	G_{IIth} (kJ/m^2)	$G_{50\%\mathrm{th}}$ (kJ/m^2)	η
0.060	0.100	0.066	2.73

The results obtained from the simulations and the experimental data are shown in Figure 12. It can be observed that the constitutive model accounts for all three regions of fatigue crack growth. In region II, where crack growth rates follow the Paris Law, it is observed that a good agreement between the predictions and the experimental data is obtained. In region I there is negligible crack growth rate for small values of the normalized energy release rate and the numerical data follows the trend of the experimental data. A significant difference between the numerical and the experimental data is observed in region III. One of the reasons for this difference is that the crack growth rates present in region III are very high and, therefore, a low-cycle instead of a high-cycle fatigue model is more appropriate for this region. However, in spite of this difference, the model can also predict Region III crack growth rate, where the Paris Law equation is not valid.

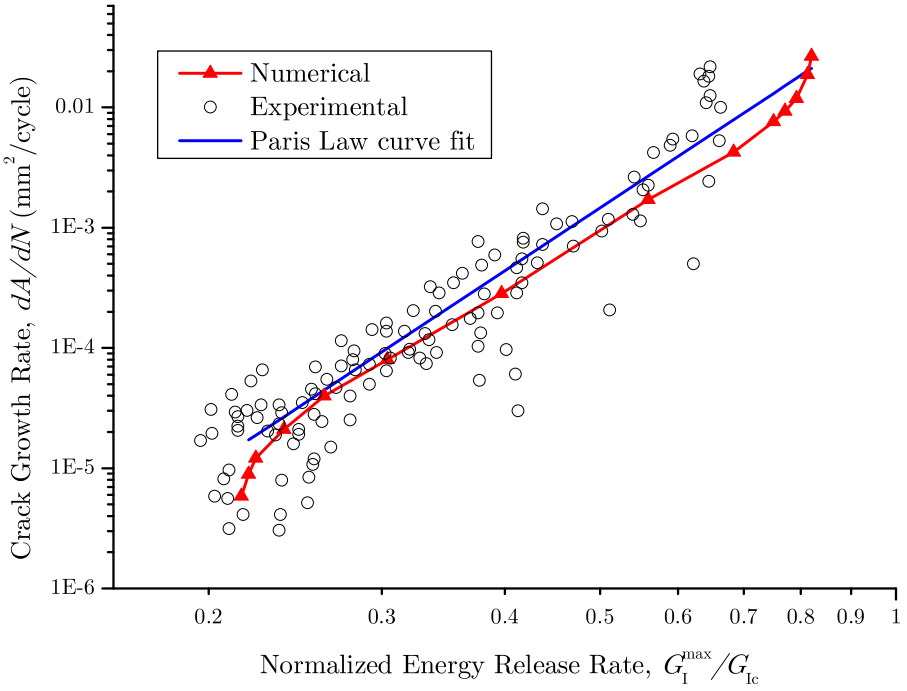

Fig. 12. *Comparison of the experimental data with the crack growth rate obtained from the numerical simulation for a Mode I DCB test.*

5.2.1 Sensitivity of the rack propagation rates to the load ratio

Several DCB tests were conducted to verify the sensitivity of the model to the load ratio. The results obtained from the simulations are shown in Figure 13 where it can be observed that higher load ratios decrease the crack growth rate.

The sensitivity of the constitutive model to the load ratio is an asset of the model. The sensitivity of the propagation rate to the load ratio derives directly from the quasi-static model rather than from a fatigue model defined as a function of the load ratio, as has been done in previous investigations [12].

It can be observed from Figure 13 that the same energy release rate threshold G_{th} is predicted for all load ratios. This result is a consequence of the current formulation of the model: the influence of the load ratio on the energy release rate threshold is not taken into account. If G_{th} is constant, then the energy release rate range threshold ΔG_{th} must vary with the load ratio, which is a trend not reflected in experimental results. To verify this dependence, the predicted crack growth rates are represented in Figure 14 as a function of the energy release rate range ΔG instead of the $G^{\max}$. It can be observed that the predicted crack growth rates for the Region II of the crack growth rate are almost independent of the load ratio, which is in agreement with experimental results [40]. However, it can also be observed that different energy release

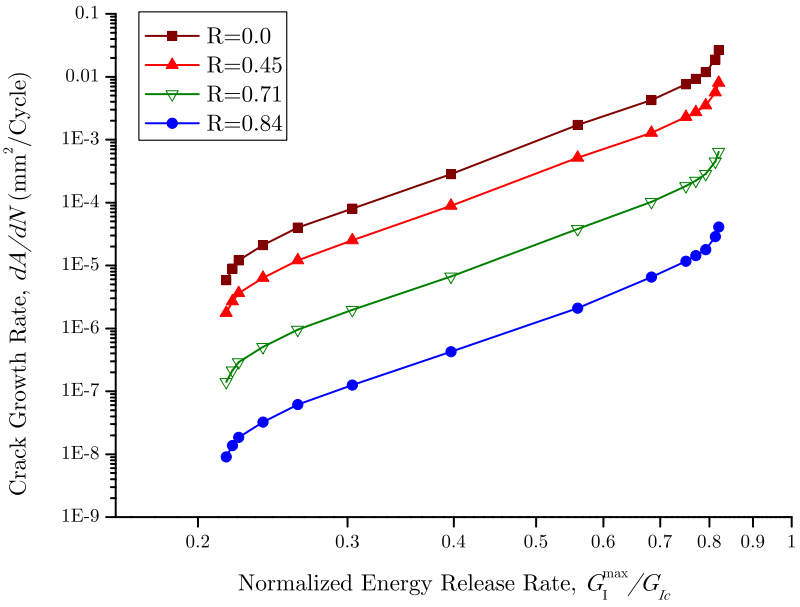

Fig. 13. *Sensitivity of the model to the load ratio for a Mode I DCB test.*

rate range thresholds are predicted for different load ratios. This effect is a limitation of the present model that will be addressed in future work by the use of the range of the energy release rate range threshold in Equation (21).

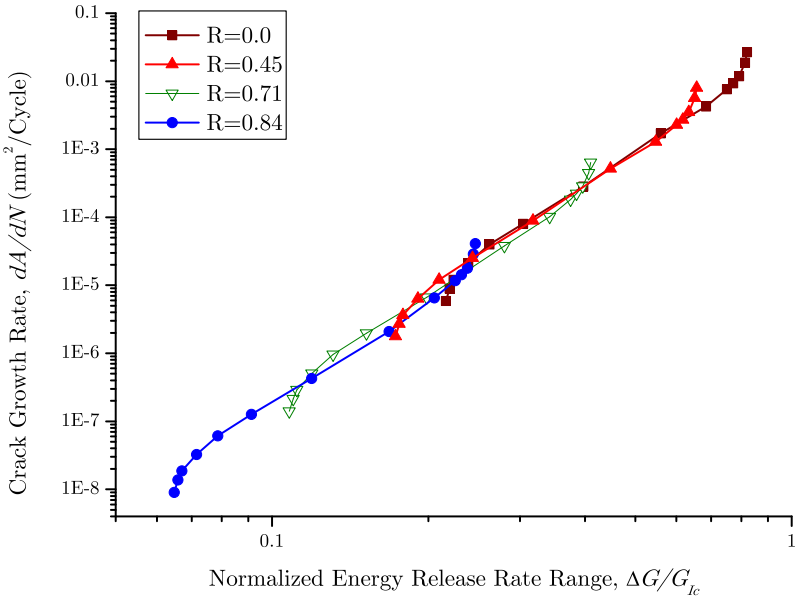

Fig. 14. *Sensitivity of the model to the load ratio for a Mode I DCB test.*

5.3 Simulation of a 4ENF test

Several tests were conducted to simulate the crack growth rate under Mode II loading for different ranges of the energy release rate. Experimental data on fatigue driven delamination growth reported in [38] was selected for comparison. The dimensions and the material of the specimen are the same used for the DCB specimen described in the previous section.

For pure Mode II, the specimen was loaded using the four point End Notched Flexure (4ENF) test shown in Figure 15. The energy release rate is related to the applied moment, $\frac{cP}{2}$, as [11]:

$$G_{\mathrm{II}} = \frac{3}{4}\frac{(\frac{cP}{2})^2}{bEI} \tag{33}$$

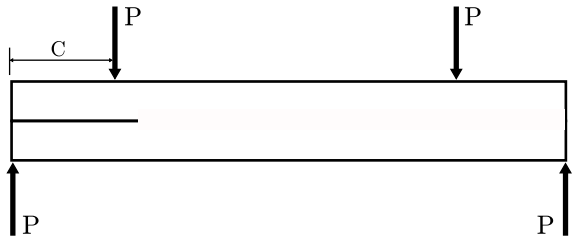

Fig. 15. *Loading pattern for Mode II 4ENF specimen.*

The finite element model used was similar to that used in the simulation of the Mode I test (see Figure 16). The Paris Law coefficients of Equation (1) were obtained from a linear regression of the experimental data presented in Ref. [38]: $C_{\mathrm{II}} = 2.99$ mm^2/cycle and $m_{\mathrm{II}} = 4.5$. The energy release rate threshold is 0.100 kJ/m^2 [38]. The fatigue properties are summarized in Table 4.

The load is applied in two steps, as described in the previous section.

The results obtained from the simulations and the experimental data [38] are shown in Figure 17. The predicted crack growth rates for small values of $\frac{G_{\mathrm{II}}^{\max}}{G_{\mathrm{IIc}}}$ are slightly higher compared to the experimental data. This difference can be attributed to friction effects that are not considered in the current implementation. Moreover, it should be mentioned that the model estimates the size of the cohesive zone using Equation (20), which may be accurate for Mode I [33] but not necessarily for Mode II. Further investigations on the estimation of the cohesive zone length under Mode II should be conducted.

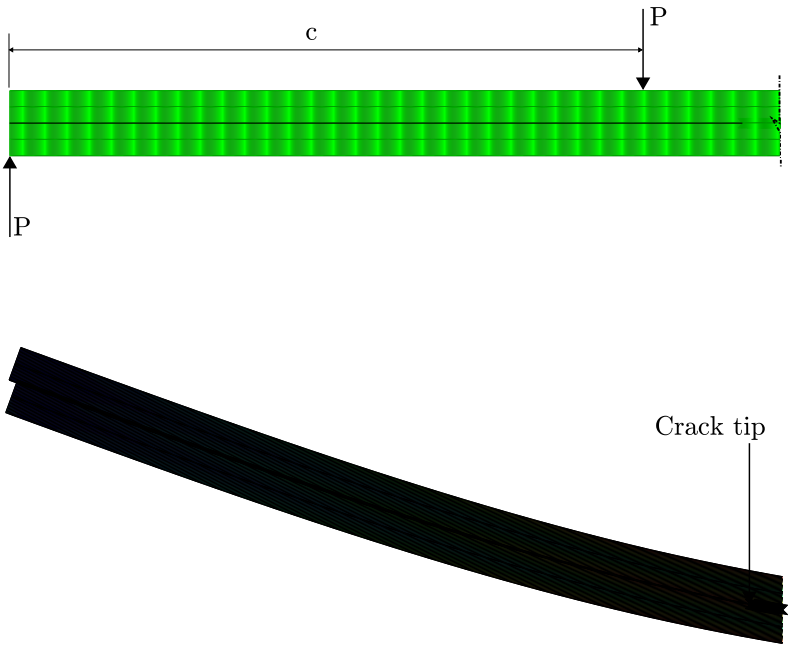

Fig. 16. *Detail of the FEM model of the 4ENF specimen.*

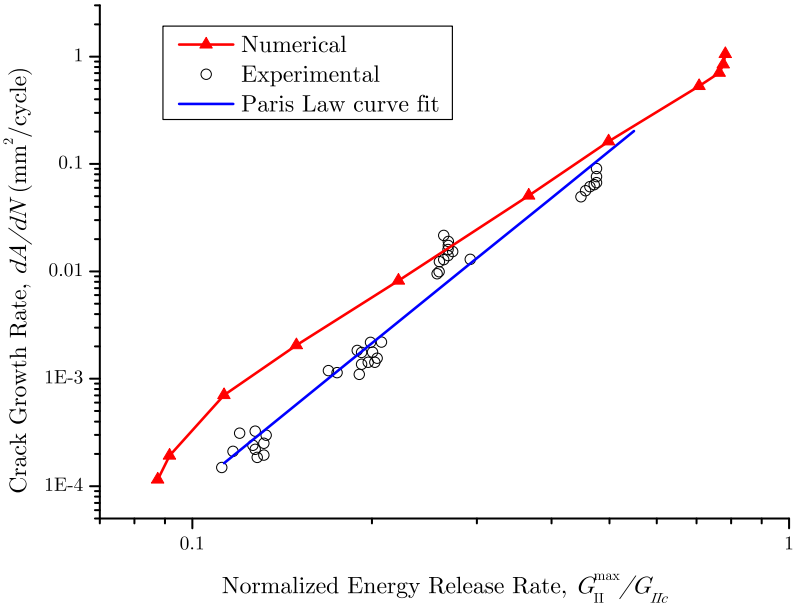

Fig. 17. *Comparison of the experimental data with the crack growth rate obtained from the numerical simulation for a Mode II 4ENF test.*

5.4 Simulation of mixed-mode loading

Several tests were conducted to simulate the crack growth rate under mixed-mode loading with $G_{\mathrm{I}} = G_{\mathrm{II}}$ for different energy release rates. Experimental data on fatigue driven delamination growth reported in [38] was selected for comparison. The dimensions and the material of the specimen are the same used for the DCB specimen described above.

For mixed-mode loading, the specimen was loaded with two moments as it is shown in Figure 18. The ratio between the two applied moments, ρ, for a mode-ratio of 50% is:

$$\rho = \frac{1 - \frac{\sqrt{3}}{2}}{1 + \frac{\sqrt{3}}{2}} \tag{34}$$

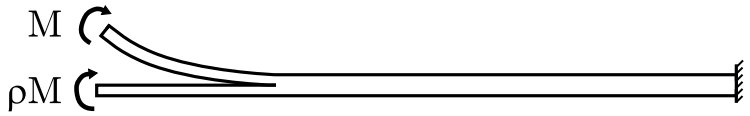

Fig. 18. *Loading pattern for mixed-mode specimen.*

The energy release rate is related to the applied moment, M, as [11]:

$$G_{\mathrm{I}} = G_{\mathrm{II}} = \frac{3}{4\left(1 + \frac{\sqrt{3}}{2}\right)^2} \frac{M^2}{bEI} \tag{35}$$

The finite element model used was similar to that used in the simulation of the Mode I test (see Figure 19).

The mixed-mode parameters C_{m}, m_{m}, and G_{th} are computed at each integration point using Equations (27), (28) and (29) to account for any changes in the mode-ratio. The fatigue material properties used in the simulation are summarized in Table 4. The load is applied in two loading steps, as described in previous sections.

The results obtained from the simulations and the experimental data [38] are shown in Figure 20. As in the case of pure Mode II, the predicted data for small values of $\frac{G^{\max}}{G_{\mathrm{c}}}$ are slightly higher than the experimental data.

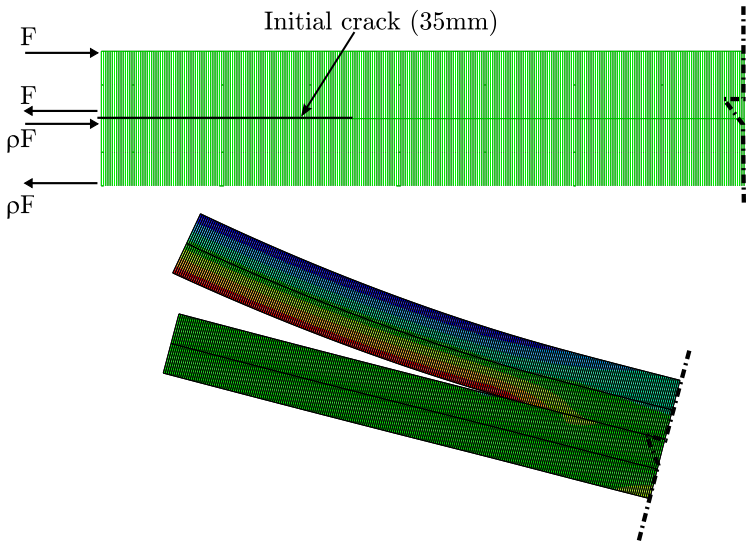

Fig. 19. *Detail of the FEM model of the specimen mixed-mode loaded.*

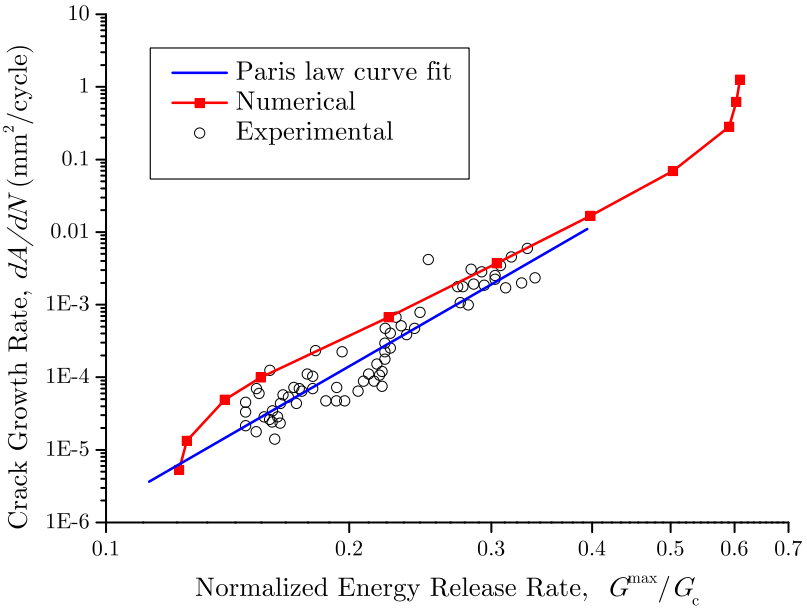

Fig. 20. *Comparison of the experimental data with the crack growth rate obtained from the numerical simulation for a mixed-mode test with* $G_I = G_{II}$.

6 Conclusions

A damage model suitable for both quasi-static and high-cycle fatigue delamination propagation was developed. The evolution of the damage variable was derived by linking Damage Mechanics and Fracture Mechanics, thus establishing a relation between damage evolution and crack growth rates. The damage evolution laws for cyclic fatigue were combined with the law of damage evolution for quasi-static loads within a cohesive element previously developed by the authors.

The model was validated using single-element numerical tests, as well as by simulating the propagation rates of Mode I, Mode II and mixed-mode tests. The model was able to reproduce the Paris Law growth rate without the need of any additional adjustment parameters. Moreover, the model accounts for the energy release rate thresholds preventing crack growth for smaller values of the energy release rate. Unlike other approaches proposed in the literature, where the dependence on the load ratio, R, is introduced through the definition of R-dependent Paris Law parameters, the effects of the load ratio on the analysis results is inherent to the formulation.

The analysis of the results indicate that the model is more accurate when Mode I loading predominates. This effect can be justified by two factors: i) friction between the crack faces is not taken into account in the model, and ii) the equation used to estimate the length of the cohesive zone was developed for for pure Mode I loading. Further investigations on the estimation of the cohesive zone length under Mode II and mixed-mode should be conducted.

In summary, the model is able to predict the crack growth rates in all regimes of propagation and the results compare favorably with the experimental data, including the negligible crack growth rates for small values of the normalized energy release rate and the sensitivity to the mode and load ratio.

7 Acknowledgments

This work has been partially funded by the Spanish government through DGICYT under contract: MAT2003-09768-C03-01.

The financial support of the Portuguese Foundation for Science and Technology (FCT) under the project PDCTE/50354/EME/2003 is acknowledged.

References

[1] P. Paris, M. Gomez, W. Anderson, A rational analytical theory of fatigue, Trend in Engineering, 13 (1961), 9–14.

[2] P. Paris, F. Erdogan, Critical analysis of propagation laws, Journal of Basic Engineering, 85 (1963), 528–534.

[3] N. Dowling, J. Begley, Fatigue crack growth during gross plasticity and the J-integral, ASTM STP 590 (1976), 82–103.

[4] D. McDowell, An engineering model for propagation of small cracks in fatigue, Engineering Fracture Mechanics, 56 (1997), 357–377.

[5] Q. Yang, D. Shim, S. Spearing, A cohesive zone model for low cycle fatigue life prediction of solder joints, Microelectronic Engineering, 75 (2004), 85–95.

[6] K. Roe, T. Siegmund, An irreversible cohesive zone model for interface fatigue crack growth simulation, Engineering Fracture Mechanics, 70 (2003), 209–232.

[7] O. Nguyen, E. Repetto, M. Ortiz, R. Radovitzky, A cohesive model for fatigue crack growth, International Journal of Fracture, 110 (2001), 351–369.

[8] V. Goyal-Singhal, E. Johnson, C.G. Dávila, Irreversible constitutive law for modeling the delamination process using interfacial surface discontinuities, Composite Structures, 64 (2004), 91–105.

[9] V. Goyal-Singhal, E. Johnson, Cohesive-decohesive interfacial constitutive law for the analyses of fatigue crack initiation and growth, 44th AIAA/ASME/ASCE/AHS Structures, Structural Dynamics, and Materials Conference AIAA-2003-1678, (2003), 1–11.

[10] R. Peerling, W. Bredelmans, R. de Borst, M. Geers, Gradient-enhaced damage modelling of high-cyclic fatigue, International Journal of Numerical Methods in Engineering, 9 (2000), 1547–1569.

[11] P. Robinson, U. Galvanetto, D. Tumino, G. Bellucci, Numerical simulation of fatigue-driven delamination using interface elements, International Journal of Numerical Methods in Engineering, 63 (2005), 1824–1848.

[12] J.J. Muñoz, U. Galvanetto and P. Robinson, On the numerical simulation of fatigue-driven delamination using interface elements, International Journal of Fatigue, 28(2006) 1136-1146.

[13] P.P. Camanho, C.G. Dávila, M. de Moura, Numerical simulation of mixed-mode progressive delamination in composite materials, Journal of Composite Materials, 37 (2003), 1415–1438.

[14] A. Turon, P.P. Camanho, J. Costa, C.G. Dávila, A damage model for the simulation of delamination in advanced composites under variable-mode loading, Mechanics of Materials, 38 (2006), 1079–1089.

[15] D. Dugdale, Yielding of steel sheets containing slits, Journal of Mechanics and Physics of Solids, 8 (1960), 100–104.

[16] G. Barenblatt, The mathematical theory of equilibrium cracks in brittle fracture, Advances in Applied Mechanics, 7 (1962), 5–129.

[17] A. Hillerborg, M. Modéer, P. Petersson, Analysis of crack formation and crack growth in concrete by means of fracture mechanics and finite elements, Cement and Concrete Research, 6 (1976), 773–782.

[18] L.M. Kachanov, Time of the rupture process under creep conditions. IZV Akad Nauk - S.S.R. Od Tech Nauk 8 (1958).

[19] O. Allix, P. Ladevèze, A. Corigliano, Damage analysis of interlaminar fracture specimens, Composite Structures, 31 (1995), 66–74.

[20] O. Allix, A. Corigliano, Modelling and simulation of crack propagation in mixed-mode interlaminar fracture specimens, International Journal of Fracture, 77 (1996), 111–140.

[21] V. Tvergaard, J. Hutchinson, The relation between crack growth resistance and fracture process parameters in elastic-plastic solids, Journal of Mechanics and Physics of Solids, 40 (1992), 1377–1397.

[22] X. Xu, A. Needleman, Numerical simulations of fast crack growth in brittle solids, Journal of Mechanics and Physics of Solids, 42 (9) (1994), 1397–1434.

[23] Needleman, A., A continuum model for void nucleation by inclusion debonding, Journal of Applied Mechanics, 54 (1987), 525–532.

[24] W. Cui, M. Wisnom, A combined stress-based and fracture-mechanics-based model for predicting delamination in composites, Composites, 24 (1993), 467–474.

[25] J. Schellekens, R. de Borst, A nonlinear finite-element approach for the analysis of mode-I free edge delamination in composites, International Journal of Solids and Structures, 30 (9) (1993), 1239–1253.

[26] U. Mi, M. Crisfield, G. Davies, Progressive delamination using interface elements, Journal of Composite Materials, 32 (1999), 1246–1272.

[27] J. Chen, M. Crisfield, A. Kinloch, E. Busso, F. Matthews, Y. Qiu, Predicting progressive delamination of composite material specimens via interface elements, Mechanics of Composite Materials and Structures, 6 (1999), 301–317.

[28] G. Alfano, M. Crisfield, Finite element interface models for the delamination analysis of laminated composites: mechanical and computational issues, International Journal for Numerical Methods in Engineering, 77 (2) (2001), 111–170.

[29] E. Reddy Jr., F. Mello, T. Guess, Modeling the initiation and growth of delaminations in composite structures, Journal of Composite Materials, 31 (1997), 812–831.

[30] M. Ortiz, A. Pandolfi, Finite-deformation irreversible cohesive elements for three-dimensional crack propagation analysis, International Journal for Numerical Methods in Engineering, 44 (1999), 1267–82.

[31] J.C. Simo, J.W. Ju, Strain and Stress-based continuum damage models-I. Formulation, International Journal of Solids and Structures, 23(23) (1987), 821–840.

[32] J. Rice, The mechanics of earthquake rupture, Physics of the Earth's Interior (Proc. International School of Physics "Enrico Fermi", Course 78, 1979; ed. A.M. Dziewonski and E. Boschi), Italian Physical Society and North-Holland Publ. Co. (1980) 555–649.

[33] A. Turon, C.G. Dávila, P.P. Camanho, J. Costa, An engineering solution for solving mesh size effects in the simulation of delamination with cohesive zone models, Engineering Fracture Mechanics, in Press.

[34] N. Blanco, E.K. Gamstedt, L.E. Asp, J.Costa, Mixed-mode delamination growth in carbon-fibre composite laminates under cyclic loading, International Journal of Solids and Structures 41 (2004), 4219–4235.

[35] Benzeggagh, M.L., Kenane, M., Measurement of Mixed-Mode delamination Fracture Toughness of Unidirectional Glass/Epoxy Composites With Mixed-Mode Bending Apparatus. Composites Science and Technology, 49 (1996), 439-49.

[36] W. Van Paepegem, J. Degrieck, Fatigue degradation modelling of plain woven glass/epoxy composites, Composites Part A, 32 (10) (2001), 1433–1441.

[37] Hibbitt, Karlsson, Sorensen, ABAQUS 6.2 Users's Manual, Pawtucket, USA (1996) .

[38] L. Asp, A. Sjögren, E. Greenhalgh, Delamination growth and thresholds in a carbon/epoxy composite under fatigue loading, Journal of Composites Technology and Research, 23 (2001), 55–68.

[39] M. Juntti, L. Asp, R. Olsson, Assessment of evaluation methods for the mixed-mode bending test, Journal of Composites Technology and Research, 21 (1999), 37–48.

[40] M. Hojo, K. Tanaka, C.G. Gustafson, R. Hayashi, Effect of Stress Ratio on Near-Threshold Propagation of Delamination Fatigue Cracks in Unidirectional CFRP, Composites Science and Technology 29 (4) (1987), 273-292.

REPORT DOCUMENTATION PAGE

Form Approved
OMB No. 0704-0188

1. REPORT DATE *(DD-MM-YYYY)*	2. REPORT TYPE	3. DATES COVERED *(From - To)*
01- 12 - 2006	Technical Memorandum	

4. TITLE AND SUBTITLE

Simulation of Delamination Propagation in Composites Under High-Cycle Fatigue by Means of Cohesive-Zone Models

5a. CONTRACT NUMBER

5b. GRANT NUMBER

5c. PROGRAM ELEMENT NUMBER

6. AUTHOR(S)

Albert Turon; Josep Costa; Pedro P. Camanho; and Carlos G. Dávila

5d. PROJECT NUMBER

5e. TASK NUMBER

5f. WORK UNIT NUMBER

7. PERFORMING ORGANIZATION NAME(S) AND ADDRESS(ES)

NASA Langley Research Center
Hampton, VA 23681-2199

8. PERFORMING ORGANIZATION REPORT NUMBER

L-19304

9. SPONSORING/MONITORING AGENCY NAME(S) AND ADDRESS(ES)

National Aeronautics and Space Administration
Washington, DC 20546-0001

10. SPONSOR/MONITOR'S ACRONYM(S)

NASA

11. SPONSOR/MONITOR'S REPORT NUMBER(S)

NASA/TM-2006-214532

12. DISTRIBUTION/AVAILABILITY STATEMENT

Unclassified - Unlimited
Subject Category 39
Availability: NASA CASI (301) 621-0390

13. SUPPLEMENTARY NOTES

An electronic version can be found at http://ntrs.nasa.gov
Turon and Costa: University of Girona; Camanho: University of Porto; Dávila: Langley Research Center

14. ABSTRACT

A damage model for the simulation of delamination propagation under high-cycle fatigue loading is proposed. The basis for the formulation is a cohesive law that links fracture and damage mechanics to establish the evolution of the damage variable in terms of the crack growth rate dA/dN. The damage state is obtained as a function of the loading conditions as well as the experimentally-determined coefficients of the Paris Law crack propagation rates for the material. It is shown that by using the constitutive fatigue damage model in a structural analysis, experimental results can be reproduced without the need of additional model-specific curve-fitting parameters.

15. SUBJECT TERMS

Fracture Mechanics; Delamination; Cohesive elements; Failure Criteria; Composite Materials

16. SECURITY CLASSIFICATION OF:			17. LIMITATION OF ABSTRACT	18. NUMBER OF PAGES	19a. NAME OF RESPONSIBLE PERSON
a. REPORT	b. ABSTRACT	c. THIS PAGE			STI Help Desk (email: help@sti.nasa.gov)
					19b. TELEPHONE NUMBER *(Include area code)*
U	U	U	UU	34	(301) 621-0390